INTERNATIONAL SOCIETY FOR
SOIL MECHANICS AND
GEOTECHNICAL ENGINEERING

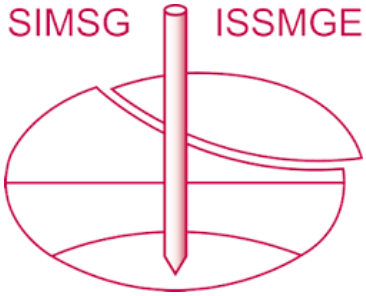

This paper was downloaded from the Online Library of the International Society for Soil Mechanics and Geotechnical Engineering (ISSMGE). The library is available here:

https://www.issmge.org/publications/online-library

This is an open-access database that archives thousands of papers published under the Auspices of the ISSMGE and maintained by the Innovation and Development Committee of ISSMGE.

Hydro-mechanical finite element modelling of rammed earth construction submitted to moisture variations

B. François & P. Gerard
Université Libre de Bruxelles, BATir Department, Brussels, Belgium

ABSTRACT: Rammed earth constructions exhibit strength and deformation properties that evolve as a function of the relative humidity of the air in contact with the walls. This work studies, through finite element simulation, the impact of the hygroscopic transfers through the wall on the structural response of a classical two-storey rammed earth building. The coupling between the mechanical and the hygroscopic behaviours is considered by the concept of effective stress for unsaturated soils. The use of this effective stress framework combined with a non-linear elasticity model together with a Drucker-Prager plastic criterion allow to reproduce the material behaviour at different suction levels. This mechanical law is coupled with a water transfer model that includes the evolution of water permeability with the degree of saturation. The simulations of the behaviour of the two-storey rammed earth building show classical deformation of the structure due to distributed load on the floors while the hygroscopic changes in the rammed earth (essentially drying) induce additional displacements of the walls that remain in a very acceptable range.

1 INTRODUCTION

Nowadays, modern experimental methods and numerical modelling open large perspectives for the development of adequate standards for rammed earth construction. Although this material demonstrates moderate mechanical performance, it remains largely sufficient for two-storey buildings. The local availability of the raw material, the low embodied energy and its potential for recycling (Morel et al. 2001) make this construction technique very attractive in the context of the development of circular economy.

Among different kinds of earthen constructions (see Houben and Guillaud 1994 for an exhaustive review), rammed earth consists of compacting successive layers of soil inside a formwork to obtain a continuous and relatively homogeneous wall formed with compacted earth. “Unstabilized” rammed earth means that there are no additional binder elements (such as cement or lime).

The strength of the construction is brought, for a part, by interlocking of soil particles induced by the compaction process that provides the required density (Gallipolli et al. 2017). Also, in addition, capillary cohesion, induced by the partial saturation of the earth, contributes, for a big part, to the resistance of the wall (Laloui et al. 2010). Consequently, the mechanical response of the unstabilized rammed earth, in terms of strength and deformability, is strongly affected by the hygroscopic conditions of the wall. As a consequence of the continuous changes of water retention conditions, the stress-strain behaviour of the wall is permanently changing and its deformation and strength must be predicted as a function of the distribution of pore pressure conditions in the wall.

Experimental studies show that the strength and the stiffness can be drastically increased when the earthen material is partially dried (Jaquin et al. 2009; Bui et al., 2014; Champiré et al. 2016). This effect of soil strengthening and stiffening is induced by internal suction that reinforces the contact between soil particles. Gerard et al. (2015) deduced a unified failure criterion based on observed strength on unconfined compression and indirect tensile tests at different suction levels. The obtained failure criterion is based on the concept of effective stress for unsaturated soils that intrinsically includes the effect of suction and water retention properties inside the stress state (Nuth and Laloui, 2008).

The link between the mechanical behaviour of the rammed earth wall (in terms of strength and deformability) and the hygroscopic conditions should be considered in the design of such a structure through an approach that considers the hygro-mechanical coupling. Hygroscopic transfers through the wall control the suction distribution which, in turn, affects the mechanical response of the structure.

Very few attempts were initiated in the last years to quantify the structural behaviour of the wall taking hygroscopic conditions into account. Up to now,

most of the approaches consider a constant and homogeneous water content profile in the whole structure (Nowamooz and Chazallon 2011). In such a way, the mechanical properties of the wall are assumed homogeneous and the transient hygro-mechanical process is totally ignored.

The present work proposes a hygro-mechanical finite element approach in order to reproduce those transient and highly non-linear processes. The computations use a consistent hygro-mechanical framework for unsaturated soils in which the stiffness and the strength are controlled by suction. Transient behaviour is taken into account through the modelling of hygroscopic transfers through the wall.

2 MATERIALS

In this study, a clayey silt soil (CL, according to the Unified Soil Classification System - USCS) that has shown its relevance for earthen construction is used. Its index properties are: liquid limit (w_L) = 32.5 %; plasticity index (IP) = 15%. The clayey fraction represents 13 %, the silty one about 61 % and the sandy one about 26 %. The large spreading of the particle size distribution provides a good interlocking of the grains, and therefore good mechanical properties. A full mechanical characterization of this clayey silt can be found in Gerard et al. (2015). Here only the most relevant results are summarized and interpreted for the calibration of material parameters needed for the hygro-mechanical computations.

For sample preparation, the soil was dynamically compacted in three layers by sequentially ramming the soil directly inside a mold of 36 mm in diameter and 72 mm in height. The compaction of each layer was achieved until the handle of the hammer "rings" when dropped onto the compacted soil, which is considered as the indication of full compaction having being attained (Hall and Djerbib 2004). The optimum water content at compaction was determined in order to obtain the highest unconfined compressive strength. Those conditions were reached for a water content of 8% and a dry density of 2000 kg/m^3. The suction of as-compacted samples, measured by the filter paper method, is equal to 2.4 MPa. From those initial conditions, different total suctions (4.17; 11.43; 22.29; 39.46; 125 MPa) were applied to the samples through the control of relative humidity by different saline solutions.

From the sample mass at equilibrium with the air relative humidity, soil water retention curve can be deduced. The equilibrium and homogeneity of water distribution was assumed to be reached when the sample mass does not change of more than 0.1% within 1 day. Figure 1 presents the soil water retention curve expressed in terms of water content, w, and degree of saturation, S_r. Only water retention properties for suctions higher than initial suction were investigated because, as it will be demonstrated in the numerical modelling, during the life of the building, the rammed earth is exclusively subject to suction higher than the initial suction of 2.4 MPa. It can be noted that the soil reaches very dry state (S_r = 12%) under ambient conditions (at 125 MPa). Water retention hysteresis upon wetting-drying was disregarded for the sake of simplicity and also because the wetting and drying curves tend to coincide for low degree of saturation (close to the residual value).

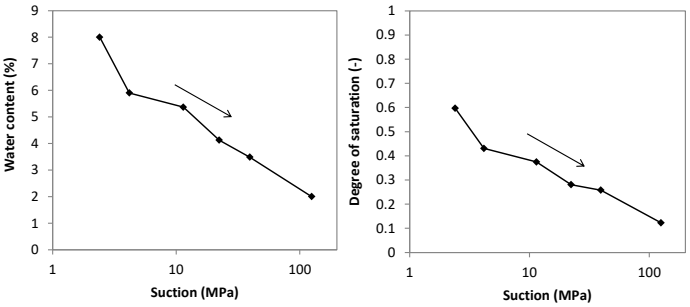

Figure 1. Soil water retention curve: suction vs. water content; suction vs. degree of saturation.

At equilibrium with surrounding relative humidity, the height and 3 diameters (bottom, middle and top) were measured with a caliper for each sample. Figure 3 presents the volumetric strain upon drying.

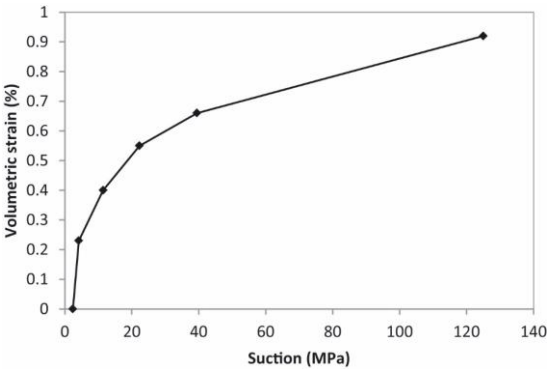

Figure 2. Contractive volumetric strain upon drying from an initial suction of 2.4 MPa.

Unconfined compression tests are performed in order to determine the unconfined compressive strength (UCS) of soil samples with unrestricted horizontal deformation. Tests were performed at different suctions described previously. The stiffness modulus was obtained as the steepest slope of the axial stress–strain curve in a strain interval of 0.2% (i.e. the slope is obtained as a finite difference between +0.1% and -0.1% of strain around the considered point). The Unconfined Compressive Strength (UCS) is taken as the maximum axial stress reached.

UCS and stiffness modulus (E) are reported as a function of suction in Figure 3. For each suction, 2 to 4 unconfined compression tests were performed. Except for the results at 4.17 MPa of suction, a logarithmic regression curve provides a good estimation of the obtained UCS and E. The low accuracy of the vapour transfer techniques at small suctions (Delage

et al. 1998) can probably explain the out-of-trend strength and stiffness measured at a suction of 4.17 MPa.

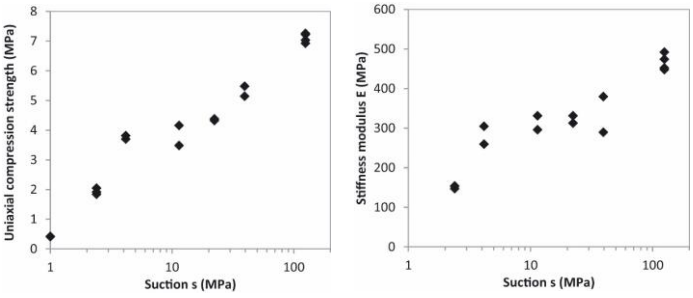

Figure 3. Unconfined compressive strength and stiffness modulus of the tested soils as a function of suction.

3 HYGRO-MECHANICAL BEHAVIOUR

3.1 *Constitutive laws*

In this work, the hygro-mechanical behaviour of the rammed earth wall is addressed through finite element computations considering mechanical stress-strain behaviour and hygroscopic transfers. The LAGAMINE finite element code, including a thermo-hydro-mechanical finite element formulation (Collin et al. 2002; Gerard et al. 2008), has been used. The complete formulation, with the details of equilibrium and balance equations as well as the water flow and vapor diffusion equations, can be found in François et al. (2017). Here only the important coupling equations are highlighted.

The mechanical behavior is governed by the effective stress for unsaturated soil σ', as a combination of the total stress σ and suction s (Bishop 1959; Nuth and Laloui 2008):

$$\boldsymbol{\sigma}' = \boldsymbol{\sigma} + \chi s\mathbf{I} = \boldsymbol{\sigma} + \left(S_r\right)^{\alpha} s\mathbf{I} \tag{1}$$

where I is the identity matrix and s the suction that is the difference between air and water pressure. In this expression, it has been decided to use a hyperbolic function of the degree of saturation S_r for the expression of the effective stress parameter χ, as suggested by Alonso et al. (2010). α is a material parameter.

The mechanical law is a Drucker-Prager elasto-plastic constitutive model with non-linear hypo-elasticity where the Young modulus E is a function of the mean effective stress through a hyperbolic function:

$$E = E_{ref}\left(\frac{p'}{p'_{ref}}\right)^{n^e} \tag{2}$$

where p' is the mean effective stress. E_{ref} is the reference Young modulus at the reference mean effective stress, p'_{ref} (= 1 MPa in our case). n^e is a material parameter.

The mechanical behaviour is elastic-perfectly plastic: the material response is fully elastic up to the Drucker–Prager failure surface:

$$f \equiv q - M\left(p' + \frac{c'}{\tan\phi'}\right) = 0 \quad \text{with} \quad M = \frac{6\sin\phi'}{3-\sin\phi'} \tag{3}$$

q is the deviatoric stress and c' and ϕ' are the effective cohesion and friction angle.

3.2 *Material parameters*

Table 1 reports the calibrated materials parameters.

Table 1. Material parameters.

Parameters	Symbols	Units	Values
Young modulus at reference mean effective stress p'_{ref} = 1MPa	E_{ref}	MPa	208
Non-linear elasticity exponent	n^e	-	0.81
Poisson coefficient	ν	-	0.25
Friction angle	ϕ'	°	36.5
Cohesion	c'	kPa	6.2
Dilatancy angle	ψ	°	0
Exponent of effective stress parameter	α	-	2.08
Coefficient for water retention curve	n_w	-	1.325
Coefficient for water retention curve	α_w	MPa	0.528
Coefficient for water retention curve	$S_{r,res}$	-	0
Coefficient of permeability	k_w^{sat}	m^2	$5.54E^{-16}$
Porosity	n	-	0.26
Tortuosity	τ	-	0.50

The parameters of the van Genuchten's water retention curve (n_w, α_w, $S_{r,res}$) have been calibrated to obtain the best fit with the experimental curve, in the least square sense. The exponent of the effective stress parameter α has been fixed at 2.08 to obtain a unified failure criterion (unaffected by suction) according to the methodology developed by Gerard et al. (2015). The two parameters of Eq. 2 (E_{ref} and n^e) are calibrated based on the elastic stiffness observed along unconfined compression tests. The best fit in the least square sense is obtained for n^e = 0.81 and E_0 = 208 MPa. The intrinsic permeability in saturated conditions has been evaluated experimentally to $5.54\ 10^{-16}$ m^2. According to van Genuchten (1980), it is assumed that the relative permeability coefficient that controls the evolution of the permeability with the degree of saturation can be directly obtained from the retention curve parameters.

4 CASE STUDY

We consider a classical two-storey building (a ground floor plus a first floor) supported by 45 cm thick rammed earth external walls with two 6 m span floors made of wood. At the connection between slabs and walls, a piece of concrete is placed to avoid stress concentration at the contact between

wood and rammed earth. Also, the base course of the wall is made of concrete on a height of 50 cm. Those construction techniques are conventional for rammed earth building (Houben and Guillaud 1994). The problem is studied in two dimensions and only half of the structure is considered for symmetry reason. Figure 4 shows the considered geometry.

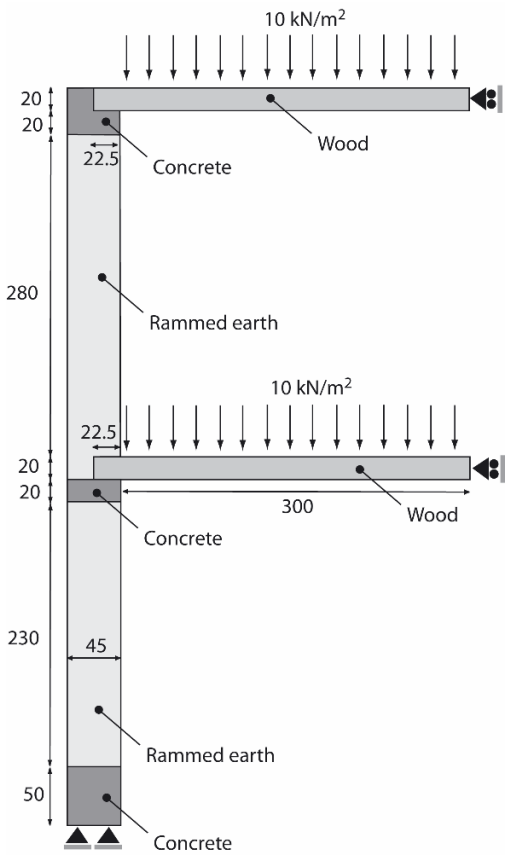

Figure 4. Considered geometry of the case study. Dimensions are in cm.

The rammed earth properties are taken from the experimental studies above (see Table 1) while the properties of concrete and wood are conventional. We neglect the hygroscopic transfers in those two materials (i.e. the governing stress is the total stress) and the mechanical response of those two materials is assumed linear elastic ($E_{concrete}$= 20 GPa; $\nu_{concrete}$ = 0.15; E_{wood} = 11 GPa; ν_{wood} = 0.25).

4.1 *Boundary conditions*

Hydraulic conditions are applied as an imposed water pressure at the wall faces. For the external conditions, the evolution of air relative humidity during the year 2014 collected in the observatory of Uccle (Belgium) is considered. To evaluate the behaviour of the structure during several years, the same annual conditions are repeated during 6 years. The simulation starts in January. The daily values evolving along the year are fitted by a bi-linear curve, as indicated in Figure 5. The internal relative humidity in the building is deduced from the external temperature, recorded in the meteorological observatory of Uccle (Belgium), according to the relation proposed by AASHRAE Tenworld (2008):

$$RH_{int} = 50 + \frac{18}{20} T_{ext} \quad (4)$$

where RH_{int} is the internal relative humidity, in percent and T_{ext} is the external temperature, in *°C*. According to AASHRAE Tenworld (2008), this relation is valid from -10°C to 20°C. Figure 6 plots the obtained internal relative humidity.

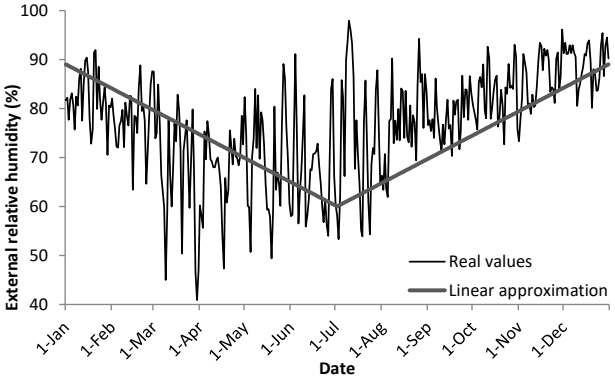

Figure 5. Daily evolution of the external air relative humidity as observed in Uccle Observatory (Belgium) during the year 2014.

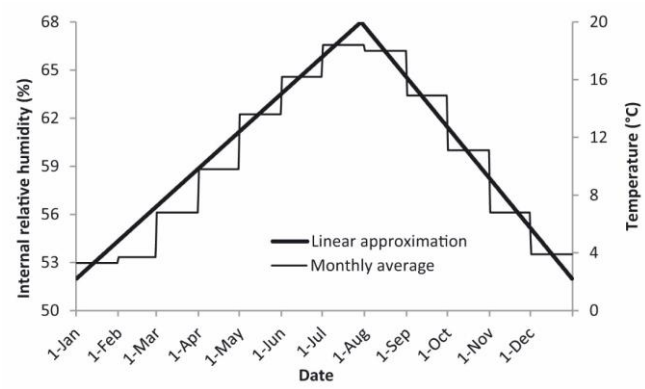

Figure 6. Linear approximation of the monthly average external temperature, as recorded at the meteorological observatory of Uccle (Belgium), and corresponding internal relative humidity.

Once the relative humidities are known on both faces of the wall, the corresponding negative water pressures can be deduced from the Kelvin's law.

The mechanical boundary conditions reproduce the fixed displacement in the horizontal and vertical directions at the level of the foundation, the fixed horizontal displacement at the symmetry axis and the uniformly distributed pressures on the floors (vertical pressure of 10 kN/m^2 corresponding to permanent and temporary loads).

The mechanical load is immediately applied at the beginning of the simulation and is maintained all along the process. So, at time t_0, the displacements in the structure are only due to the mechanical loading (10 kN/m^2 on each floor) and then the displacements evolve due to the evolution of the hydraulic conditions in the structure induced by climatic changes on both faces of the wall.

4.2 *Results*

In summer, the external environment is dry (s = 69 MPa; RH = 60%) while the internal condition is wetter (s = 52 MPa; RH = 68%). In winter, the conditions are reversed: s = 16 MPa (RH = 89%) and s = 88 MPa (RH = 52%) for external and internal conditions, respectively. Consequently, the wall is continuously submitted to hygroscopic changes. Figure 7 shows the profile of the suction through the wall at a height of 5 meters in January and July during the 6 years of simulation. During the first years of simulation, the suction in the core of the wall increases significantly because the environmental conditions are much dryer than the initial conditions of the rammed earth after compaction. Then, after a few years, the core of the wall is still drying but more gently while the suction changes are still noticeable near the external face, on a skin of around 5 cm thickness. Time required to reach a constant hygroscopic condition in the middle of the wall depends on the permeability of the soil, the thickness of the wall and the climatic conditions.

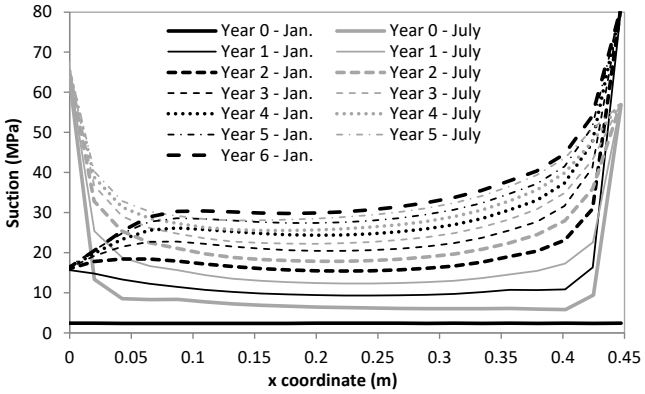

Figure 7. Profile of suction through the wall at a height of 5 meters in January and June during 6 years.

In terms of displacements, the uniformly distributed pressure on the floors produces a deflection of the structure induced by the bending of the slabs and the wall. The maximum vertical displacement at mid-span induced by the distributed load is 1.84 cm for the top floor and 1.29 cm for the bottom floor. The connections between slab and wall slightly rotate due to the flexibility of the wall. Then, the global drying of the rammed earth along the 6 years of simulation produces a shrinkage of the materials that generates an additional vertical displacement of the structure increasing from the bottom to the top. Consequently, the 1.84 cm of displacement induced by the distributed pressure on the floors at time t=0 increases up to 3.23 cm after 6 years due to rammed earth shrinkage (Figure 8).

Figure 9 shows the evolution of the vertical displacement at the mid-span of the two floors during the 6 years of simulation. After the initial deflection due to the immediate mechanical loading, the displacement still increases due to shrinkage of the wall. However, this process tends progressively to stabilize because the suction change in the core of the wall is slower with time. Small oscillations are observed due to the annual cycles of the environmental conditions.

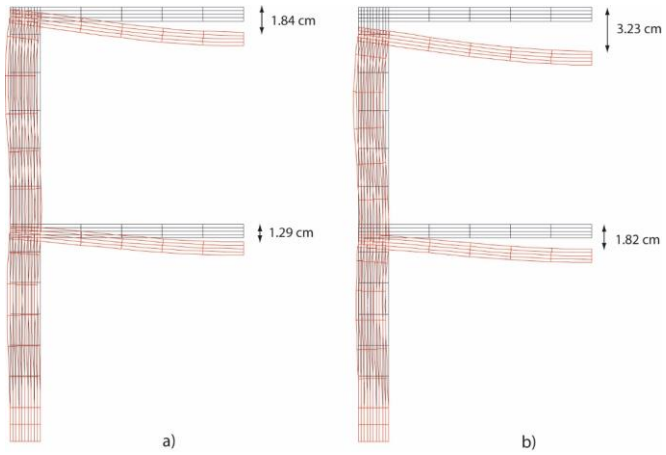

Figure 8: Deformed structure (a) after the application of the pressure on floors at time t=0 and (b) at the end of the 6th year of simulation. Amplification of the displacement: 20.

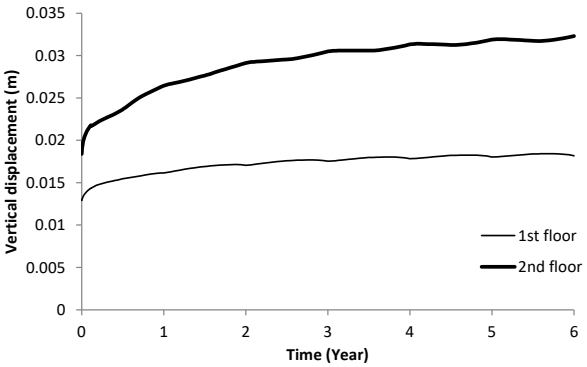

Figure 9. Evolution of the vertical displacements at the mid-span of the two floors.

All along the process, the structure is really far from failure. Figure 10 shows the plastic indicator *PI* that is the ratio between the current deviatoric stress and the deviatoric stress corresponding to failure for the same mean effective stress:

$$PI = \frac{q}{q_{failure}} \tag{6}$$

This parameter is a local indicator of how far the considered point is from failure. When *PI=1*, the stress state is upon the failure criterion. As demonstrated in Figure 10, the plastic indicator remains lower than 0.5 all along the process. After the loading of the floors (Figure 10a), the maximum *PI* are located at the top of the wall close to both faces. This is due to the bending of the wall that generates uniaxial tension and compression on the sides of the wall. Then, in the bulk of the wall, the plastic indicator is increased between time t=0 (*PI = 0.08*) and after 6 years of simulation (*PI =0.2*). This is due to the gradient of suction in the wall that produces a gradi-

ent of effective stress which in turn induces deviatoric stress. Also, at the connection between the wall and the first floor (Figure 10b), the PI values are slightly increased because the differential shrinkage between rammed earth and wood produces some shear stresses. However, the PI values remain in very acceptable limits everywhere.

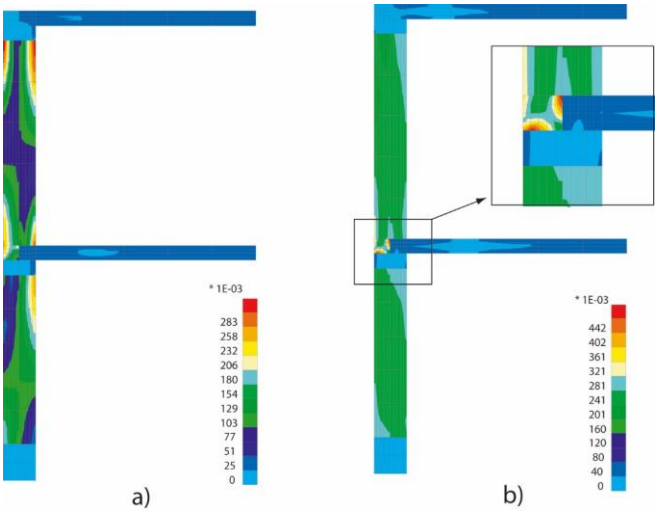

Figure 10: Map of plastic indicator in the structure (a) after the application of the pressure on floors at time t=0 and (b) at the end of the 6th year of simulation for the standard loading (10 kN/m^2 on the floors).

5 CONCLUSIONS

It is essential to characterize the hygroscopic behaviour of rammed earth construction because it has a strong influence on the structural response of the rammed earth wall, in terms of deformation and potential failure. This coupled hygro-mechanical behaviour in a rammed earth wall has been addressed through finite element computations. The mechanical behaviour is directly coupled to the hygroscopic conditions through the effective stress for unsaturated soils. Non-linear elasticity takes into account the stiffening of the material when it is dried.

The hygro-mechanical model has been calibrated based on relatively conventional soil mechanics laboratory tests (unconfined compression tests at different controlled suctions and shrinkage measurements upon drying).

A typical two-storey rammed earth building has been considered as a case study. The problem has been addressed in two dimensions. A uniform load of 10 kN/m^2 applied on the floors produces classical bending and contraction of the walls without local failure. Additionally, the hygroscopic changes in the wall produce further settlements induced by the material drying that remain in a very acceptable range. It is observed that the structure is continuously evolving because of the endless change of the hygroscopic environmental conditions but the global trend is essentially drying during the 6 first years, in a Belgian climate.

6 REFERENCES

AASHRAE TenWolde 2008. Standard 160P: criteria for moisture control design analysis in buildings. *ASHRAE Transactions*, 114(1) : 167–169

Alonso, E.E., Pereira, J.M., Vaunat, J. & Olivella, S. 2010. A microstructurally based effective stress for unsaturated soils. *Géotechnique* 60(12): 913-925.

Bishop, A.W. 1959. The principle of effective stress. *Tecnisk Ukeblad*, 39: 859-863.

Bui, Q.B., Morel, J.C., Hans, S. & Walker, P. 2014. Effect of moisture content on the mechanical characteristics of rammed earth. *Construction and Building Materials* 54: 163-169.

Champiré, F., Fabbri, A., Morel, J.C., Wong, H. & McGregor F. 2016. Impact of relative humidity on the mechanical behavior of compacted earth as a building material. *Construction and Building Materials* 110: 70-78.

Chandler, R.J. & Gutierrez, C.I. 1986. The filter paper method of suction measurement. *Géotechnique* 36(2): 265–268.

Collin, F., Li, X., Radu, J.P. & Charlier, R. 2002. Thermo-hydro-mechanical coupling in clay barriers. *Engineering Geology* 64:179–93.

Delage, P., Howat, M. & Cui, Y. 1998. The relationship between suction and swelling properties in a heavily compacted unsaturated clay. *Engineering Geology* 50(1-2): 31-48.

Drucker, D.C. & Prager, W. 1952. Solid mechanics and plastic analysis for limit design. *Quarterly of Applied Mathematics* 10(2): 157–165.

François, B. Palazon, L. & Gerard, P. 2017. Structural behaviour of unstabilized rammed earth constructions submitted to hygroscopic conditions. *Construction and Building Materials* 155: 164-175.

Gallipoli, D., Bruno, A.W., Perlot, C. & Mendes, J. 2017. A geotechnical perspective of raw earth building. *Acta Geotechnica*. DOI: 10.1007/s11440-016-0521-1.

Gerard, P., Mahdad, M., McCormack, A.R. & François B. 2015. A unified failure criterion for unstabilized rammed earth materials upon varying relative humidity conditions. *Construction and Building Materials* 95: 437-447.

Gerard, P., Charlier, R., Chambon, R. & Collin, F. 2008. Influence of evaporation and seepage on the convergence of a ventilated cavity. *Water Resources Research* 44(5).

Hall, M.R. & Djerbib, Y. 2004. Rammed earth sample production: context, recommendations and consistency. *Construction and Building Materials.* 18: 281-286.

Houben, H. & Guillaud, H. 1994. *Earth construction - A comprehensive guide, Second Edition*. Intermediate Technology Publications. London, UK.

Jaquin, P.A., Augarde, C.E., Gallipoli, D. & Toll D.G. 2009. The strength of unstabilised rammed earth materials. *Géotechnique* 59(5): 487–490.

Laloui, L., Nuth, M. & François B. 2010. Mechanics of unsaturated soils. *In: Mechanics of unsaturated materials, Eds. L. Laloui*, Wiley & Sons, Inc. 29-54

Morel, J.C., Mesbah, A., Oggero, M. & Walker P. 2001. Building houses with local materials: means to drastically reduce the environmental impact of construction. *Building and Environment* 36: 1119–26.

Nowamooz, H. & Chazallon, C. 2011. Finite element modelling of a rammed earth wall. *Construction and Building Materials* 25(4): 2112-2121.

Nuth, M. & Laloui L. 2008. Effective stress concept in unsaturated soils: clarification and validation of a unified framework. *International Journal for Numerical and Analytical Methods in Geomechanics* 32(7): 771-801.

van Genuchten, M.T. 1980. A closed-form equation for predicting the hydraulic conductivity of unsaturated soils. *Soil Science Society of America Journal* 44: 892–898.